scientific reports

OPEN

Dipole antenna incorporated with metasurface and cavity reflector for wideband circular polarisation and high gain

Cho Hilary Scott Nkimbeng[1], Heesu Wang[1], Hakjune Lee[1], Yong Bae Park[1,2]✉ & Ikmo Park[1]✉

This paper presents the design of a low-profile dipole antenna incorporating a polarisation converter metasurface and cavity reflector for wideband circular polarisation and high-gain performance. The antenna comprises a modified dipole structure with two parasitic patches placed on the bottom side of the substrate in a coplanar configuration, and a metasurface comprising four modified square metal patches in a 2 × 2 layout, with a centrally positioned cross-shaped strip printed on the top side of the substrate. A modified cavity reflector with truncated corners and four triangular extensions at the top corners of the cavity was introduced beneath the dipole to enhance gain. Each unit cell of the metasurface included a complementary patch structure formed by etching two diagonally oriented C-shaped slots onto a square metal patch, resulting in a distinct chiseled pattern. These diagonal slots are critical for generating a 90° phase difference and balancing the amplitude of the orthogonal polarisation components, thus facilitating the conversion from linear to circular polarisation. The proposed antenna achieves a global bandwidth of 49.7% (4.0–6.73 GHz), simultaneously satisfying impedance matching, axial ratio, and gain requirements with a peak gain of 10.8 dBic and a radiation efficiency exceeding 92%.

Keywords Circular polarisation, Dipole antenna, Low profile, Metasurface, Global bandwidth, Polarisation converter

The development of satellite communication systems has created a significant demand for high-gain circularly polarised (CP) antennas. These CP antennas are gaining increasing attention because of their ability to prevent polarisation mismatches and mitigate multipath effects[1–8]. To meet this demand, several methods have been explored for designing high-gain CP antennas[9–24]. Metasurfaces have emerged as efficient solutions for generating CP waves among the approaches. These structures offer unique capabilities for polarisation manipulation, allowing precise control over the amplitude and phase of both the reflected and transmitted waves. This capability has paved the way for developing effective metasurface-based polarisation converters[25–27].

Several configurations have been explored for enhancing the performance of CP antennas using metasurfaces. One widely studied approach involves Fabry–Pérot resonators, where an air gap between a linearly polarised (LP) radiator and a metasurface polarisation converter enables constructive interference at specific frequencies. This setup effectively increases the CP gain and extends the axial ratio (AR) bandwidth, as shown in various high-gain CP antenna designs[9–13]. In[9] the authors presented a high-gain Fabry–Pérot CP antenna. The design featured an LP patch antenna and a unit-cell polarisation converter comprising a combination of an LP square patch on the bottom substrate layer and a truncated patch on the top substrate layer of the polarisation converter, with both patches connected by a via. Although the antenna achieved a very high gain, it exhibited narrow impedance and AR bandwidths, as well as low efficiency. In[10] the authors designed a Fabry–Pérot antenna for C-band satellite communication. The LP radiator was a truncated patch, and a Z-shaped metasurface was used for linear polarisation (LP: this acronym can be used interchangeably with linearly polarised) to circular polarisation (CP: this acronym can be used interchangeably with circularly polarised) conversion. They achieved high gain and wide impedance bandwidth but yielded low AR bandwidth, low efficiency, poor radiation patterns at higher frequencies, and a thick profile size. In addition, the authors of[11] presented a high-gain Fabry–Pérot CP antenna utilizing a patch array excited by a feeding network and chessboard polarisation converter. Although they

[1]Department of Electrical and Computer Engineering, Ajou University, Suwon 16499, Republic of Korea. [2]Department of AI Convergence Network, Ajou University, Suwon 16499, Republic of Korea. ✉email: yong@ajou.ac.kr; ipark@ajou.ac.kr

achieved high gain, the design had limitations, including narrow impedance and AR bandwidths. Moreover, the radiation patterns obtained were poor, and the antenna had a bulky profile size. In[12] the authors presented a dual-CP high-gain Fabry–Pérot antenna based on a dual–polarised LP patch radiator and a metasurface polarisation converter comprising a circular patch etched with a slot oriented at 45° for LP-to-CP conversion. They achieved high gain, albeit with extremely narrow impedance and AR bandwidths. In addition, the efficiency was low, and the radiation patterns were poor. In[13] the authors designed a high-gain CP Fabry–Pérot antenna based on a double-differential-feed-patch LP source and highly reflective metasurface polarisation converter comprising two corner-cut truncated patches with orthogonal slots and twelve shorted pins. They achieved high gain with extremely narrow impedance and AR bandwidths, as well as a thick profile.

Other studies have explored alternative approaches for high-gain CP antennas with polarisation converter metasurfaces. One method involves placing a transmissive metasurface polarisation converter above an LP source with an air gap[14–15] while another uses a reflective metasurface polarisation converter beneath the LP source with an air gap[16,17]. These configurations enable the metasurface to convert LP waves into CP waves, enhance CP performance, and support improved bandwidth and gain characteristics.

Both designs using the Fabry–Pérot technique and placing reflective metasurfaces with an air-gap separation between the LP source and converter have limitations of poor radiation characteristics, bulky profile sizes, and narrow impedance and AR bandwidths, necessitating further study in this area. To this end, cavity-backed antennas are promising candidates for high-efficiency and high-gain wireless communication systems. In[18] the authors proposed a double-cavity structure for high-efficiency, high-gain CP antennas. The LP source was placed on the top side of the feeding cavity at the lower side with a feeding slot, and 3×3 and 8×8 periodic radiating cross slots were positioned on the top side of the upper cavity to convert the LP waves to CP waves. Although the structure achieved high gain and efficiency, it resulted in a narrow AR bandwidth and bulky profile owing to its double-cavity design.

This paper presents a novel approach to achieve high gain, high efficiency, wide impedance, and AR bandwidths by incorporating a modified dipole antenna with a wideband complementary-shaped LP-to-CP converter metasurface and cavity reflector. The antenna comprises a modified dipole structure with two parasitic patches in a coplanar configuration on the bottom side of the substrate and a metasurface with four modified square metal patches arranged in a 2×2 layout with a centrally positioned cross-shaped strip on the top side of the substrate. A modified cavity reflector featuring truncated corners and four triangular extensions at the top corners was introduced beneath the dipole to focus energy in the broadside direction. The proposed antenna achieves a global bandwidth of 4.0–6.64 GHz, simultaneously satisfying impedance matching, AR, and gain requirements. Specifically, it offers an AR bandwidth of 49.7% (4.01–6.73 GHz), an impedance bandwidth of 67.3% (3.50–7.05 GHz), a 3-dB gain bandwidth of 61.1% (3.68–6.92 GHz), a peak gain of 10.8 dBic at 5.2 GHz, and a radiation efficiency exceeding 92%. With compact dimensions of $80 \times 80 \times 15.508$ mm³ ($1.36 \times 1.36 \times 0.26$ λ_o^3 at 5.1 GHz), the antenna is suitable for wideband applications in satellite and wireless communications.

Antenna geometry

The geometry of the proposed antenna, as illustrated in Fig. 1a, incorporates a cavity structure along with a metasurface and modified dipole fed by a tapered balun. The antenna is designed on a Rogers AD250C substrate with dimensions of $80 \times 80 \times 15.508$ mm³ corresponding to $1.36 \times 1.36 \times 0.26$ λ_o^3, where λ_o is the center frequency of the AR bandwidth at 5.1 GHz. This substrate has a relative permittivity (ε_r) of 2.5 and loss tangent ($tan\delta$) of 0.0015, supporting high-frequency operation with minimal loss. The metasurface, located on the top side of the substrate, comprised four modified square metal patches arranged in a 2×2 layout with periodicity P_m. A cross-shaped strip with dimensions W_c and L_c for its width and length, respectively, was placed at the center of the 2×2 metasurface structure to improve impedance and AR matching, as shown in Fig. 1b. Each unit cell comprises a metal patch modified by two diagonal C-shaped slots into the metal to create a chiseled pattern. These slots, with widths g_1 and g_2, are separated by d_1 and d_2, providing a 90° phase shift and equalizing the amplitude between the orthogonal components of the incident LP wave, thereby enabling CP radiation. The gap of each metal patch is denoted as g_m. The primary radiator, which is a modified dipole with stepped-width arms and vertical stubs, was positioned at the bottom of the substrate in a coplanar configuration, as shown in Fig. 1c. The structure comprises modified dipole arms with a fork-like stub for impedance matching and two parasitic patches that improve both impedance matching and the AR bandwidth. The dimensions of the modified dipole arm include L_f (length) and W_f (width of the feeding part), and L_d and W_d represent the length and width of the entire arm, respectively, which together determine the resonance frequency of the antenna. Additionally, the fork-shaped adjustment at both ends of the dipole, with length L_n and width W_n, acts as a notch, further improving impedance matching and contributing to the wideband performance of the antenna. A vertical rectangular structure of length L_{st} and width W_{st} was added to each dipole arm, aiding in current distribution and impedance matching. The two parasitic patches have widths of W_p and lengths of L_p, which further aid in improving the impedance matching. Figure 2a shows the standard cavity reflector, and Fig. 2b depicts the modified cavity reflector with truncated corners and four triangular extensions at the top corners of the cavity. Figure 2c shows a 3D view of the metasurface dipole antenna incorporating a modified cavity reflector. The cavity was placed beneath the metasurface dipole antenna, as shown in Fig. 1a and 2d. The dimensions of the cavity are $W \times W \times h_{cav}$, where the lengths and widths of the cavity are the same as that of the substrate of the metasurface dipole antenna, but the cavity height h_{cav} is different from the substrate height h_s, as shown in Fig. 1a. The cavity enhances the gain by focusing the radiated energy and reducing the backward radiation, resulting in a more concentrated broadside radiation pattern. This is achieved by suppressing surface wave propagation and unwanted modes, thereby improving the radiation efficiency and polarisation purity. With its truncated corners and triangular extensions, the modified cavity further refined energy confinement and redirection, enhancing the front-to-back ratio and reducing the scattering effects. These modifications improved the surface current
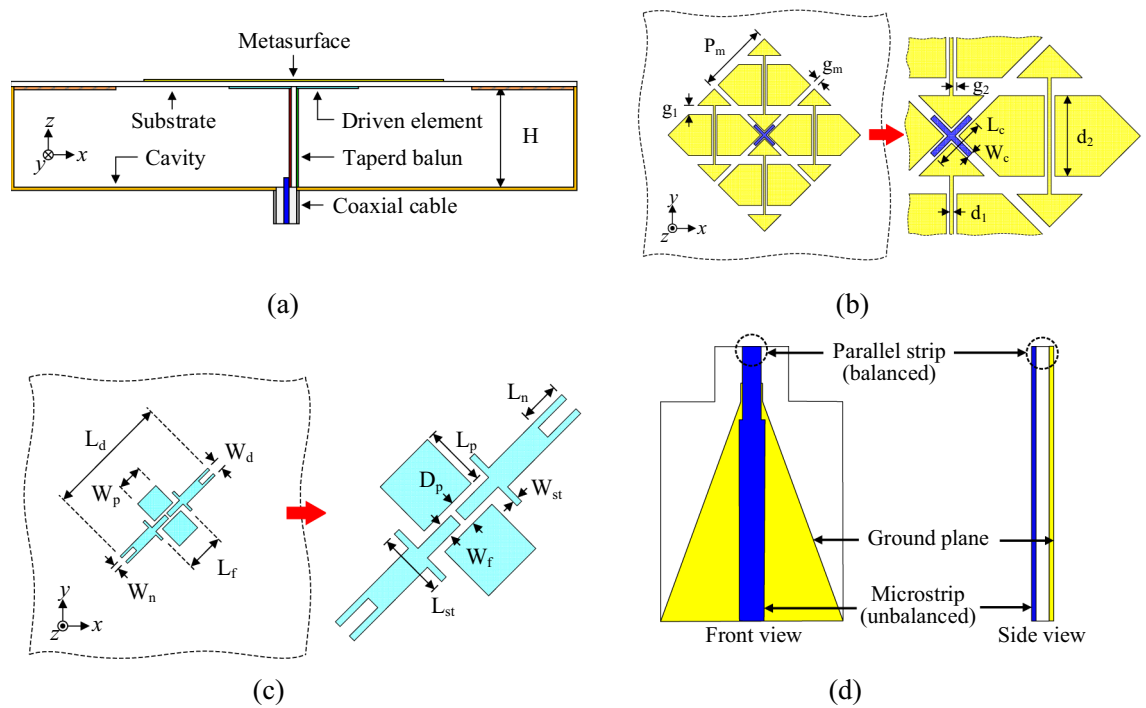
Fig. 1. Antenna geometry: (**a**) side view of dipole antenna incorporated with the metasurface and cavity, (**b**) top view of the top side of the metasurface, (**c**) top view of the modified dipole antenna, and (**d**) microstrip-to-parallel strip tapered balun.
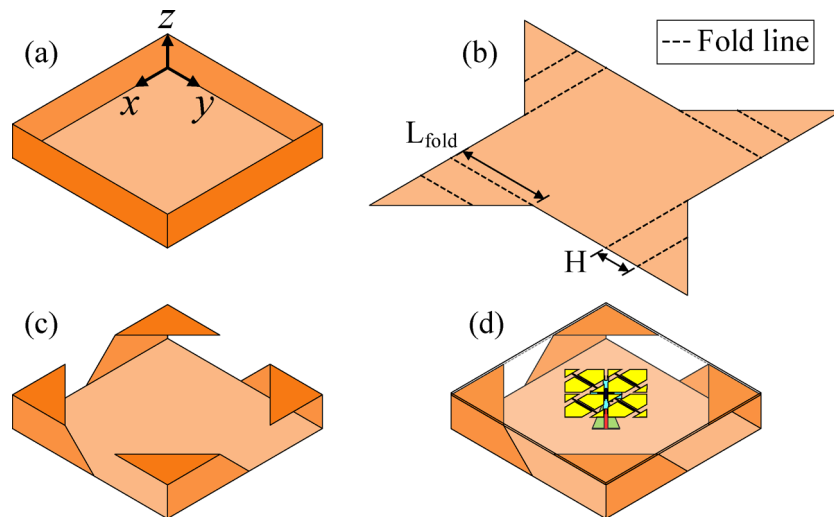

Fig. 2. (**a**) Conventional cavity reflector, (**b**) unfolded 2D structure, (**c**) modified cavity structure with truncated corners and triangular extensions at the top corners, and (**d**) 3D view of the proposed structure.

control and polarisation characteristics, resulting in superior gain and AR performance compared to those of the standard cavity. The antenna is excited using a tapered microstrip-to-parallel stripline balun[4] which transforms the unbalanced input from the coaxial feed into a balanced differential signal across the dipole arms,

as shown in Fig. 1d. Specifically, the inner conductor of the coaxial cable connects to one dipole arm via a vertical stripline, while the outer conductor is soldered to the opposite dipole arm through a wide vertical ground plane, achieving balanced excitation. This structure ensures effective impedance matching and current symmetry, which are essential for achieving circular polarisation over a wide bandwidth.

The antenna was optimised using an ANSYS high-frequency structure simulator (HFSS) to obtain a wide AR bandwidth, good impedance matching, and a low profile. The optimised design parameters are as follows: $W = 80$ mm, $P_m = 15.6$ mm, $g_m = 1.0$ mm, $g_1 = 1.8$ mm, $g_2 = 0.2$ mm, $d_1 = 0.2$ mm, $d_2 = 9.2$ mm, $L_d = 24$ mm, $W_d =$

2 mm, L_f = 8 mm, W_c= 0.6 mm, L_c =6 mm, W_f = 1 mm, L_{st} = 8 mm, W_{st} = 0.5 mm, L_n = 2 mm, W_n = 1 mm, L_p = 6 mm, W_p = 4 mm, h_s = 0.508 mm, and h_{cav} = 15 mm.

The design guidelines of the proposed antenna are as follows:

1. The modified dipole arms, placed in a coplanar configuration on the bottom of the substrate, established the resonant frequency of the antenna. A vertical stub was introduced to improve impedance matching.
2. A complementary-shaped wideband LP-to-CP conversion metasurface was designed with periodicity P_m and placed on the top of the substrate to convert the LP waves from the dipole antenna into CP waves. The diagonally oriented C-shaped slot had widths g_1 and g_2 separated by d_1 and d_2. These slots were designed to create a 90° phase shift between the orthogonal polarisation components and achieve a near-equal amplitude, thereby improving the CP over a wide frequency band.
3. To enhance both the impedance matching and AR bandwidths, two parasitic patches were introduced close to the modified dipole arms. These patches have a width W_p and length L_p, positioned strategically to strengthen the coupling and ensure optimal current distribution. Additionally, a cross-shaped strip was centrally placed within the 2 × 2 metasurface structure to further improve the impedance matching and AR performance.
4. A modified cavity reflector was positioned beneath the metasurface dipole-antenna structure. This reflector enhances the gain by reducing backward radiation and focusing energy in the broadside direction. The modifications, including truncated corners and triangular extensions, further improved the energy confinement, front-to-back ratio, and overall radiation performance.
5. Finally, the performance of the antenna, including the bandwidth, gain, and efficiency, was optimised through careful fine-tuning of the metasurface polarisation converter, modified dipole structure, parasitic patches, tapered balun, and modified cavity reflector. This comprehensive optimisation ensures wide AR and impedance bandwidths, enhanced gain owing to the cavity structure, and high efficiency with minimal loss across the operating frequency range.

Antenna design evolution

The design evolution was thoroughly analysed across four antenna configurations (Ants I, II, III, and IV) to provide comprehensive insights into the operating mechanism of the proposed high-gain CP antenna. Ant I comprises only a modified dipole LP source without parasitic patches, as shown in Fig. 3a. Ant II comprises a modified dipole incorporated with a 2 × 2 complementary-.

shaped LP-to-CP polarisation converter metasurface without parasitic patches, as depicted in Fig. 3b. Ant III includes a modified dipole LP source with a complementary 2 × 2 metasurface structure[28,29] and two parasitic patches along with a centrally positioned cross-shaped strip, as illustrated in Fig. 3c. Ant VI includes Ant III, which has a modified cavity reflector with truncated corners and four triangular extensions at the top corners of the cavity reflector, as shown in Fig. 3d.

Comparative analyses of the reflection coefficient ($|S_{11}|$), gain, and AR characteristics were conducted for various configurations (Ants I, II, and III) and the proposed antenna (Ant IV). Ant I achieves a limited impedance bandwidth ranging from 4.46 to 5.21 GHz (15.5%), a peak gain of 2.2 dBic, and an AR > 70 dB, as shown in Figs. 4a,b and c, respectively. Ant I does not generate CP because it operates solely as an LP source. Ant II was incorporated into a 2 × 2 complementary-shaped LP-to-CP converter metasurface on Ant I, as shown in Fig. 4b. This modification introduces additional resonances, resulting in multiple impedance frequency bands: 3.18 to 3.58 GHz (11.8%), 4.15 to 4.67 GHz (11.8%), and 7.64 to 9.58 GHz (18.8%), as shown in.

Figure 3a; and an AR < 7 dB across 3 to 6.8 GHz and an AR < 3 dB between 4.1 and 4.39 GHz (6.8%), as illustrated in Fig. 4b. The modified antenna, Ant II, achieves a peak gain of 3.2 dBic, as shown in Fig. 4c, which corresponds to an approximately 1-dB gain improvement compared to that of Ant I. Additionally, the CP performance of Ant II is enabled by the introduction of the polarisation converter metasurface, which facilitates a 90° phase difference and near-equal amplitude between the two orthogonal polarisation components of the incoming LP wave from the dipole antenna, resulting in CP radiation. Despite these enhancements, the impedance and AR bandwidths remained relatively narrow, because most of the structures were not fully matched across the entire frequency range. To address the limitations of narrow impedance and AR bandwidths in Ant II, parasitic elements were strategically positioned to interact with the main radiating structure and improve impedance matching. This improvement occurred because the strategically positioned parasitic elements[30,31] acted as secondary resonators coupled with the primary radiating structure. This coupling introduced additional resonant modes near the main resonance, effectively broadening the impedance bandwidth by creating multiple resonant paths. Additionally, a cross-shaped strip was introduced to enhance the AR matching and obtain Ant III. The additions of the parasitic elements and cross-shaped strip led to significantly improved performance with an impedance bandwidth from 3.52 to 8.42 GHz, corresponding to an 83% fractional bandwidth, a wide 3-dB AR bandwidth from 4.2 to 6.5 GHz (43.39%), and a peak gain of 3.4 dBic, as shown in Figs. 4a, b, and c, respectively. Although the aforementioned antenna design, Ant III, demonstrates good impedance and CP performance, it exhibits very low gain, limiting its suitability for applications requiring high-gain CP. To address this limitation, a cavity reflector was introduced to improve the gain and overall performance of the antenna. The standard cavity reflector was modified by truncating the corners and adding four triangular extensions to the top corners to obtain the proposed Ant IV structure. First, truncating the corners alters the current path along the edges, preventing the formation of unwanted surface currents. This effectively reduces energy loss and scattering, allowing more energy to be confined and directed towards the broadside direction, thereby improving the gain and radiation efficiency. Additionally, the triangular extensions at the top corners help fine-tune the current distribution on the cavity reflector, further stabilizing the radiation characteristics across the operational frequency band. Thus, the proposed antenna (Ant IV) achieves an impedance bandwidth of
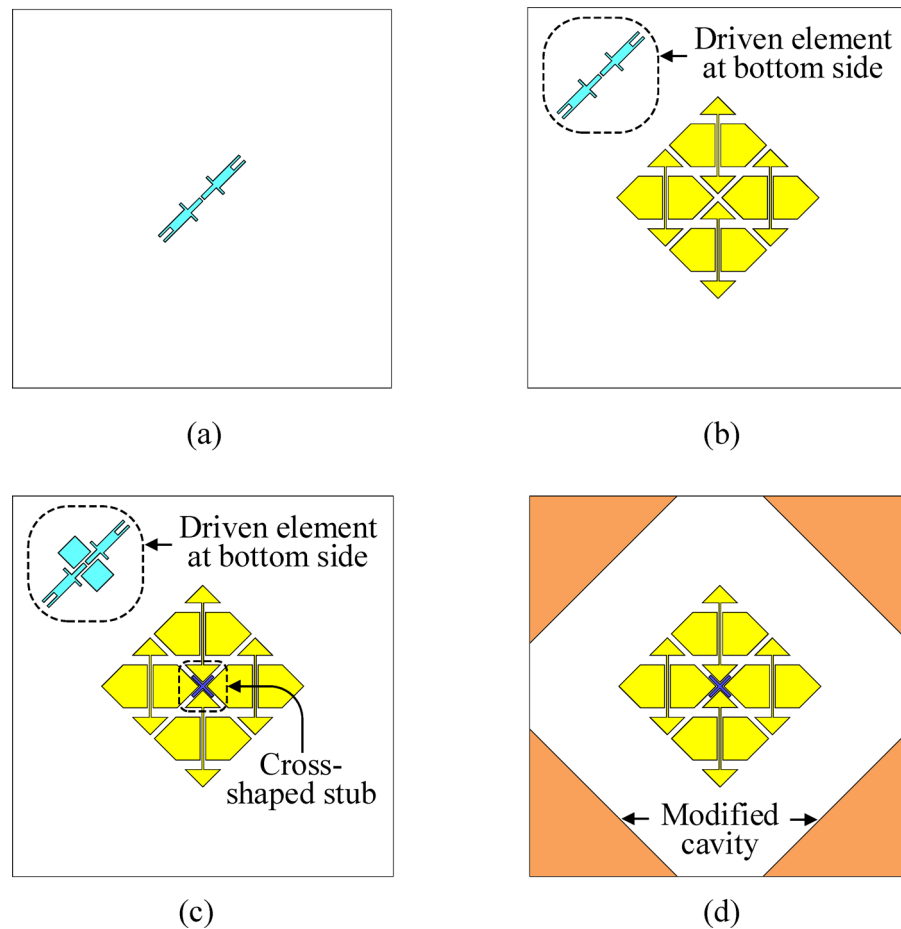
Fig. 3. Antenna design evolution: (**a**) Ant I, (**b**) Ant II, (**c**) Ant III, and (**d**) Ant IV.
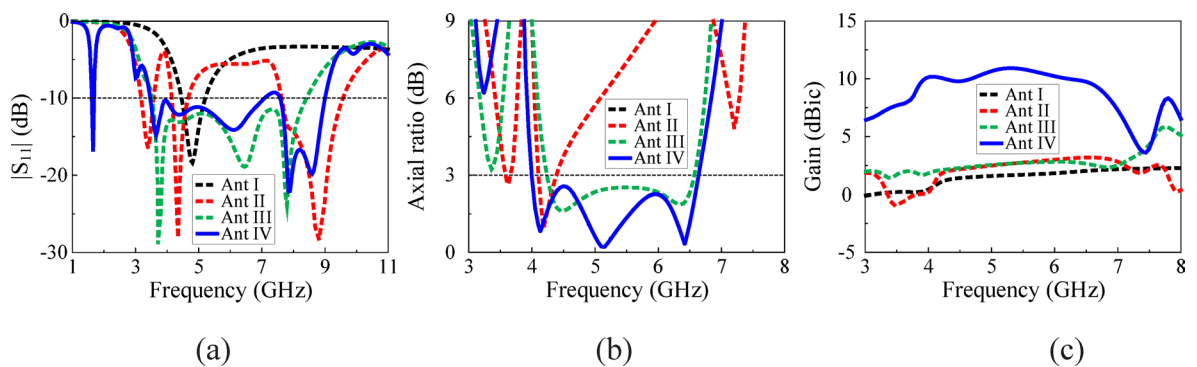

Fig. 4. Antenna performance comparison: (**a**) reflection coefficient, (**b**) axial ratio, and (**c**) gain.

68.8% (3.46–7.09 GHz), a wide AR bandwidth of 49.2% (4.01–6.64 GHz), and an improved peak gain of 10.9 dBic, as shown in Figs. 4a, b, and c, respectively. Overall, the proposed antenna exhibited excellent performance compared to Ants I, II, and III, achieving high-gain and wideband CP response.

Experimental results

To validate the performance of the proposed design, a low-profile dipole antenna incorporating a metasurface and cavity reflector was fabricated and measured. The fabricated prototype is shown in Fig. 5. S-parameter measurements were performed using an Agilent N5230A network analyser with a 3.5-mm coaxial calibration standard (GCS35M). Far-field measurements were performed at the RFID/USN Center in Incheon, South Korea, within a fully anechoic chamber using an Agilent E8362B network analyser. A standard wideband horn antenna was used as the transmitter, and the proposed metasurface-based antenna with a cavity reflector was used as
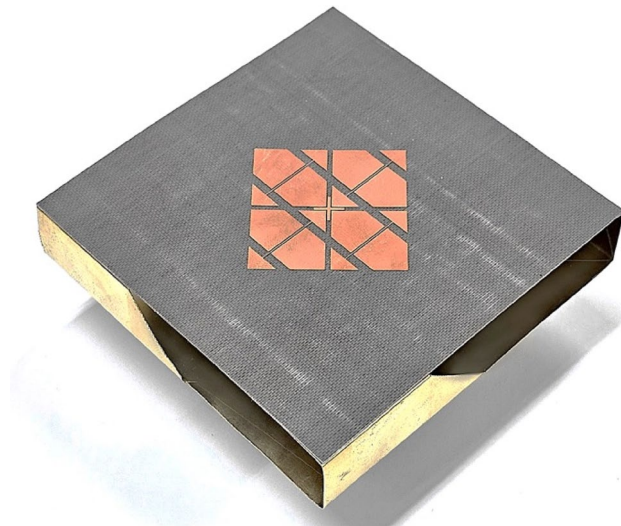
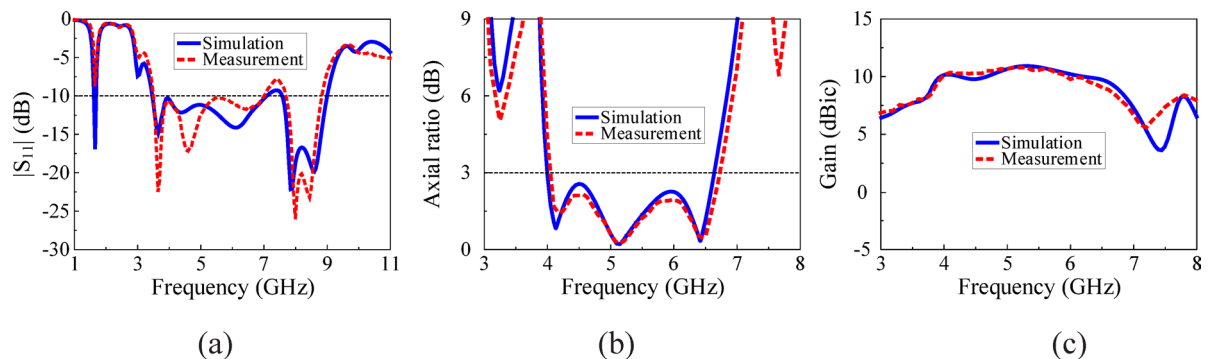**Fig. 5**. Fabricated sample of the proposed antenna.

Fig. 6. Simulated and measured: (**a**) reflection coefficient, (**b**) axial ratio, and (**c**) gain.

the receiver. The antennas were positioned 7-m apart to satisfy the far-field criteria. During measurements, the proposed antenna was rotated from − 180° to 180° at 0.5°/s with a 1° scan angle, while the horn antenna remained stationary. The AR was determined by recording the received power over the full rotation and computing the ratio of the major to minor axes of the resulting polarisation ellipse. The 3 dB AR bandwidth was defined as the frequency range over which the AR remained below 3 dB, indicating effective circular polarisation. The measured results aligned closely with the simulated data, with only minor discrepancies, likely caused by slight fabrication misalignments. Figure 6a shows the measured and simulated reflection coefficients of the fabricated antenna. The measured impedance bandwidth for $|S_{11}| < - 10$ dB was 3.48 to 7.08 GHz (68.8%), which is similar to the simulated impedance bandwidth of 3.50 to 7.05 GHz (67.3%). Figure 6b shows a comparison of the measured and simulated AR bandwidths of the proposed antenna. The simulated AR bandwidth was 4.03–6.64 GHz (49.2%), and the measured AR bandwidth was 4.05–6.73 GHz (49.7%). The measured and simulated gain performances of the proposed antenna are shown in Fig. 6c. The simulated peak gain reaches 10.9 dBic at 5.2 GHz, whereas the measured peak gain was slightly reduced to 10.8 dBic in the broadside direction. The measured and simulated radiation patterns are shown in Figs. 7 and 8, and 9. As shown in Figs. 7 and 8, and 9, respectively, the measured and simulated radiation patterns at 4.1, 5.1, and 6.4 GHz show unidirectional radiation with LHCP in the broadside direction. Furthermore, the cross-polarisation levels remained significantly low, indicating the effective suppression of the right-hand CP components and confirming the high purity of the LHCP pattern across the operating frequencies. These results validate the suitability of the proposed antenna for applications requiring stable unidirectional LHCP radiation.

Performance comparison

Table 1 provides a detailed performance comparison between the proposed antenna and other notable high-gain CP designs based on metasurfaces reported in the literature[9–17]. The selection criteria for the comparison table included the antenna profile size, − 10-dB impedance bandwidth, 3-dB AR bandwidth, 3-dB gain bandwidth, peak gain, and efficiency. In[10] the authors achieved a high-profile structure (0.51 λ_o), whereas the proposed design is approximately half the size with a profile size of 0.26 λ_o. The impedance bandwidth of the proposed design
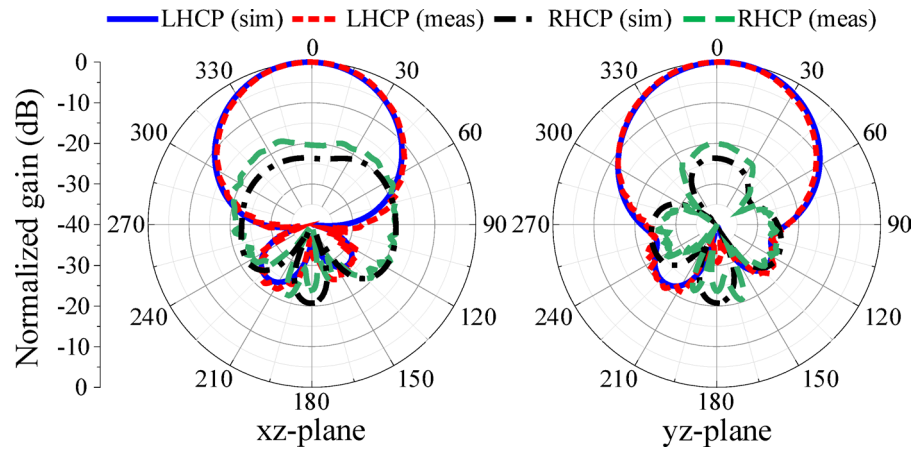
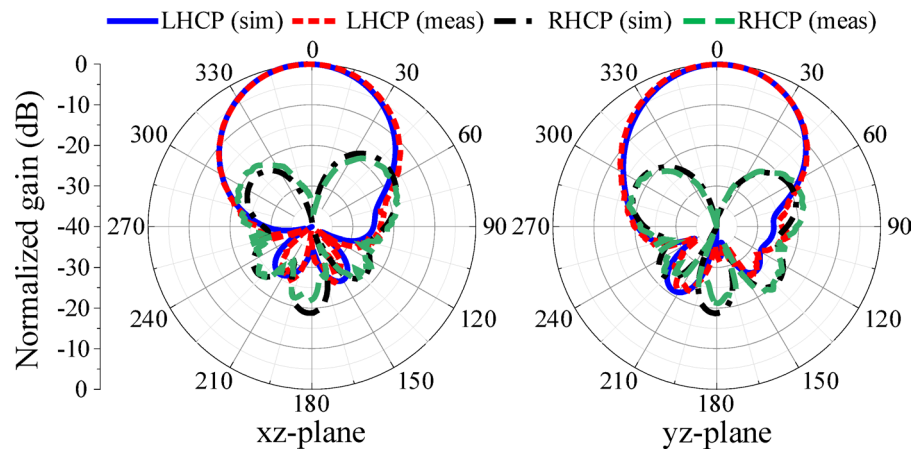Fig. 7. Radiation pattern at 4.1 GHz: (**a**) xz-plane and (**b**) yz-plane.

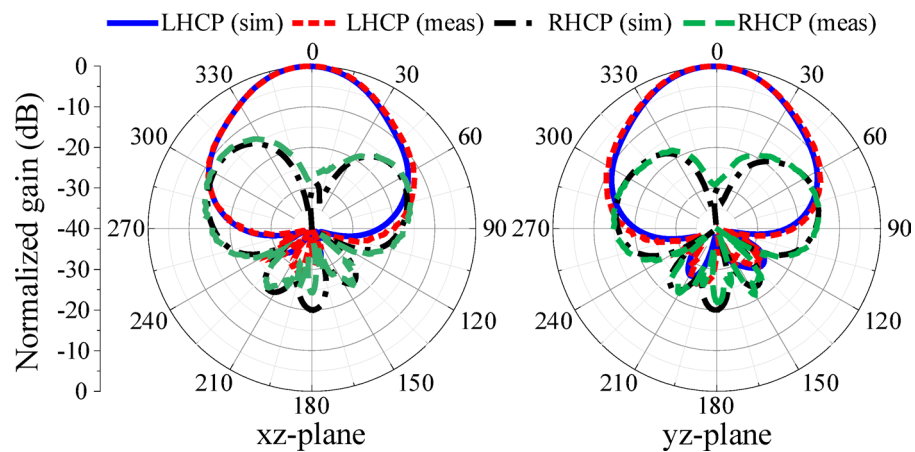Fig. 8. Radiation pattern at 5.1 GHz: (**a**) xz-plane and (**b**) yz-plane.

Fig. 9. Radiation pattern at 6.4 GHz: (**a**) xz-plane and (**b**) yz-plane.

(68.8%) is similar to the 64% bandwidth presented in[10]. The AR bandwidth of the proposed design (49.7%) was significantly greater than the 18% reported in[10]. The peak gain achieved in[10] (12.88 dBic) is higher than the proposed design by 10.9 dBic, but the 3-dB gain bandwidth of 30% is narrower than that of the proposed design by 61.1%. The authors in[13] achieved a profile size of 0.58 λ_o, which was thicker than that of the proposed

Ref.	Size^3 (λ_o^3)	-10 dB IBW (%)	3 dB ARBW (%)	Peak gain (dBic)	3 dB gain BW (%)	Efficiency (%)	Technique
10	1.5×1.5×0.51	64	18	12.88	30	65	Fabry–Pérot
13	2.4×2.4×0.58	11.3	8.6	13.7	13.8	80	Fabry–Pérot
14	2.16×2.16×0.6	8.6	7.1	12.5	—	—	Superstrate PCM + LP source
15	0.98×0.98×0.12	15.7	13	9.6	28.5	85	Superstrate PCM + LP source
16	—	63	8.2 10.7	8.0	—	—	Reflective metasurface +LP source
17	1.62×1.62×0.32	14.3	8.0 7.1	8.49	22.2	—	Reflective metasurface + LP source
18	1.33×1.33×0.52	1.6	0.5	12.6	2	94	Cavity + slot PCM
Proposed	1.36×1.36×0.26	68.8	49.7	10.8	61.1	92	Cavity +dipole incorporated with PCM

Table 1. Performance comparison of the proposed antenna with other antenna designs. λ_o: the free-space wavelength corresponding to the center frequency of the AR bandwidth.

design. Additionally, the proposed design achieved a wider impedance and AR bandwidths of 68.8% and 49.7%, respectively, compared to that in[13] (11.3% and 8.6%). Although the gain in[13] 13.7 dBic is higher than that of the proposed structure.

(10.9 dBic), the structure in[14] has a relatively narrow 3-dB gain bandwidth (13.8%). The proposed design achieves a lower profile size compared to that presented in[14] (0.60 λ_o). Additionally, the impedance bandwidth in[14] was only 8.6%, which was considerably narrower than that of the proposed design. The AR bandwidth of the proposed antenna (49.7%) was also significantly wider than the 7.1% in[14]. The peak gain in[14] (11.5 dBic) was only 0.6 dB higher than that of the proposed design (10.9 dBic). In[15] the design achieves a better profile size (0.12 λ_o) compared to the proposed design (0.26λ_o). However, its impedance bandwidth is much narrower (15.7%) than that of the proposed design (68.8%). Additionally, the AR bandwidth achieved in[15] has extremely narrow (13%) compared to that of the proposed design (49.7%). Moreover, the peak gain achieved in[15] (9.6 dBic) is lower than that of the proposed design (10.9 dBic), and its 3 dB gain bandwidth (28.5%) is also narrower than that of the proposed design (61.1%). The proposed design also exhibits a higher radiation efficiency of 92% compared to the 85% reported in[15]. The authors in[16] did not specify the profile size, but the proposed design offered a wide impedance bandwidth of 68.8% compared to 63% in[16]. Additionally, the dual-band AR bandwidths achieved in[16] of 8.2 and 10.7% were considerably narrower than the 49.7% AR bandwidth of the proposed design. The peak gain in[16] (8.0 dBic) is 2.9 dB lower than the proposed design of 10.9 dBic. Additionally, the.

gain variation in[16] is severe compared to that of the proposed design. The proposed antenna provides a lower profile (0.26 λ_o) compared to that reported in[17] (0.32 λ_o). Additionally, the impedance bandwidth of the proposed design (68.8%) is also significantly broader than that of 14.3% in[17]. Furthermore, the AR bandwidth in[17] was only 8.0%, which was significantly narrower than that of the proposed design of 49.7%. The design in[17] achieved a peak gain of 8.03 dBic, which is slightly lower than that of the proposed design at 10.9 dBic. Lastly, the antenna design in[17] had a profile size of 0.52 λ_o, which is twice as large as that of the proposed design. Additionally, the impedance bandwidth in[18] is extremely narrow (1.6%) compared to the proposed design. Furthermore, the AR bandwidth in[18] was only 0.5%, significantly smaller than that of the proposed design. In[17] the peak gain of 12.6 dBic is higher than that of the proposed design (10.9 dBic). However, the 3-dB gain bandwidth in[18] is about 2%, which is extremely narrow compared with the 61.1% offered by the proposed antenna. Additionally, a slightly higher efficiency of 94% is reported[17] whereas the proposed design achieves 92%.

Overall, the proposed design provides a lower profile size, wider impedance and AR bandwidth compared to those of the antennas in[10,13,14,16–18]. Although the design in[15] provides a lower profile size and smaller lateral size compared to the proposed design, it suffers from limited impedance bandwidth, narrow AR bandwidth, low gain, and a reduced 3-dB gain bandwidth. The gains of the designs in[10,13,14,18] are higher than that of the proposed design, however, the proposed structure offers a wider 3-dB gain bandwidth. These exceptional characteristics make the proposed design suitable for applications requiring compact size and wideband performance.

Conclusion

In this study, a low-profile dipole antenna incorporating a polarisation converter metasurface and cavity reflector was designed and analysed for wideband CP and high-gain performance. The proposed antenna achieves excellent performance characteristics, including a global bandwidth of 49.7% (4.05–6.73 GHz), satisfying impedance matching, AR, and gain requirements. It offers a wide AR bandwidth of 49.7% (4.05–6.73 GHz), an impedance bandwidth of 68.8% (3.48–7.08 GHz), and a 3-dB gain bandwidth of 61.1% (3.68–6.92 GHz). Including a modified cavity reflector with truncated corners and triangular extensions enhances the gain by minimising the unwanted radiation and focusing energy in the broadside direction. This results in a gain increase of approximately 7 dB. Its compact design, with dimensions of $80 \times 80 \times 15.508$ mm^3 ($1.36 \times 1.36 \times 0.26$ λ_o^3 at 5.1 GHz), makes it well suited for wideband applications, including satellite and wireless communications.

The effective incorporation of the metasurface and cavity reflector validated the ability of the proposed design to achieve wideband CP and high-gain performance.

Data availability

The datasets used and/or analysed during the current study available from the corresponding author on reasonable request.

References

1. Choi, S. W. & Sung, Y. Simple dual-feed dual-circular polarization antenna with high isolation. *J. Electromagn. Eng. Sci.* **23**, 154–164 (2023).
2. Li, W., Xue, W., Li, Y., Chung, K. L. & Huang, Z. A wideband differentially fed circularly polarized slotted patch antenna with a large beamwidth. *J. Electromagn. Eng. Sci.* **23**, 512–520 (2023).
3. Park, S., Qu, L., Park, M. S. & Jung, K. Y. Design of a circularly polarized planar monopole antenna with a simplified radiator structure for UWB applications. *J. Electromagn. Eng. Sci.* **24**, 145–150 (2024).
4. Wang, H., Park, Y. B. & Park, I. Design of a broadband circularly polarised uniplanar crossed-dipole antenna. *Sci. Rep.* **14**, 7821 (2024).
5. Wang, H., Byun, G., Park, Y. B. & Park, I. Circularly polarized wideband uniplanar crossed-dipole antenna with folded striplines and rectangular stubs. *IEEE Access.* **11**, 63252–63260 (2023).
6. Wang, H. & Park, I. Compact wideband circularly polarized dipole antenna using modified quadrature hybrid couplers. *IEEE Trans. Antennas Propag.* **69**, 8896–8901 (2021).
7. Nkimbeng, C. H. S., Wang, H. & Park, I. Coplanar waveguide-fed bidirectional same-sense circularly polarized metasurface-based antenna. *J. Electromagn. Eng. Sci.* **21**, 210–217 (2021).
8. Nkimbeng, C. H. S., Wang, H., Byun, G., Park, Y. B. & Park, I. Non-uniform metasurface integrated circularly polarized end-fire dipole array antenna. *J. Electromagn. Eng. Sci.* **23**, 29–41 (2023).
9. Xie, P., Wang, G., Li, H., Liang, J. & Gao, X. Circularly polarized Fabry–Perot antenna employing a receiver-transmitter polarization conversion metasurface. *IEEE Trans. Antennas Propag.* **68**, 3213–3218 (2020).
10. Supreeyatitikul, N., Boonpoonga, A. & Phongcharoenpanich, C. Z-shaped metasurface-based wideband circularly polarized Fabry–Pérot antenna for C-band satellite technology. *IEEE Access.* **10**, 59428–59441 (2022).
11. Chen, Q. & Zhang, H. High-gain circularly polarized Fabry–Pérot patch array antenna with wideband low-radar-cross-section property. *IEEE Access.* **7**, 8885–8889 (2019).
12. Wang, Y. & Zhang, A. Dual circularly polarized Fabry–Perot resonator antenna employing a polarization conversion metasurface. *IEEE Access.* **9**, 44881–44887 (2021).
13. Le, H. D., Le-Huu, T., Nguyen, K. K. & Ta, S. X. Dual circularly polarized Fabry–Perot antenna using single-layer self-polarizing PRS. *IEEE Antennas Wirel. Propag. Lett.* **22**, 2575–2579 (2023).
14. Zhang, X., Chen, C., Jiang, S., Wang, Y. & Chen, W. A high-gain polarization reconfigurable antenna using polarization conversion metasurface. *Prog Electromagn. Res. C.* **105**, 1–10 (2020).
15. Sheersha, J. A., Nasimuddin, N. & Alphones, A. A high gain wideband circularly polarized antenna with asymmetric metasurface. *Int. J. RF Microw. Comput. Aided Eng.* **29**, e21740 (2019).
16. Mao, C., Yang, Y., He, X., Zheng, J. & Liu, T. Design of high-gain dual-band dual-circular-polarised antenna using reflective metasurface. *Electron. Lett.* **53**, 1448–1450 (2017).
17. Wang, Y. & Ge, Y. Novel single/dual circularly polarized antennas based on polarization-conversion reflective metasurfaces. *Prog Electromagn. Res. C.* **108**, 237–251 (2021).
18. Chen, R. S. et al. Circularly-polarized cavity-backed slot antenna array with simplified feeding structure. *Int. J. RF Microw. Comput. Aided Eng.* **31**, e22859 (2021).
19. Zhou, E., Cheng, Y., Chen, F. & Luo, H. Wideband and high-gain patch antenna with reflective focusing metasurface. *Int. J. Electron. Commun.* **134**, 153709 (2021).
20. Liu, Z. et al. A low-RCS, high-GBP Fabry–Perot antenna with embedded chessboard polarization conversion metasurface. *IEEE Access.* **8**, 80183–80194 (2020).
21. Cao, W., Lv, X., Wang, Q., Zhao, Y. & Yang, X. Wideband circularly polarized Fabry–Perot resonator antenna in Ku-band. *IEEE Antennas Wirel. Propag. Lett.* **19**, 586–590 (2019).
22. Xie, P. & Wang, G. Circularly polarized Fabry–Perot antenna with well RCS reduction property. *Int. J. RF Microw. Comput. Aided Eng.* **32**, e23527 (2022).
23. Li, K., Liu, Y., Jia, Y. & Guo, Y. J. A circularly polarized high-gain antenna with low RCS over a wideband using chessboard polarization conversion metasurfaces. *IEEE Trans. Antennas Propag.* **65**, 4288–4292 (2017).
24. Nasimuddin & Chia, M. Y. W. Metasurface with unequal spacing unit-cells based antenna for linear and circular polarizations. In *Proceedings of the 17th European Conference on Antennas and Propagation (EuCAP)*, Florence, Italy, 1–5 (2023).
25. Nkimbeng, C. H. S. et al. Ultra-wideband ultra-thin transmissive linear to circular polarization converter based on crossed-dipole-shaped metasurface. *IEEE Access.* **12**, 120337–120346 (2024).
26. Nkimbeng, C. H. S., Wang, H., Yoon, D., Park, Y. B. & Park, I. Single-layer dual wideband linear to circular polarisation converter with integrated parasitic elements. *Sci. Rep.* **14**, 26237 (2024).
27. Supreeyatitikul, N., Lertwiriyaprapa, T. & Phongcharoenpanich, C. S-shaped metasurface wideband circularly polarized patch antenna for C-band applications. *IEEE Access.* **9**, 23944–23955 (2021).
28. Nkimbeng, C. H. S., Wang, H. & Park, I. Low-profile dipole antenna integrated with wideband polarization converter. *IEEE Int. Workshop Antenna Technol. (iWAT)*, 1–3 (2025).
29. Nkimbeng, C. H. S., Wang, H., Park, Y. B. & Park, I. Wideband circularly polarized metasurface-integrated dipole antenna for bidirectional applications. Submitted for publication.
30. Ta, S. X., Kedze, K. E., Chien, D. N. & Park, I. Bandwidth-enhanced low-profile antenna with parasitic patches. *Int. J. Antennas Propag.* 6529060 (2017).
31. Kedze, K. E., Wang, H., Ta, S. X. & Park, I. Wideband low-profile printed dipole antenna incorporated with folded strips and corner-cut parasitic patches above the ground plane. *IEEE Access.* **7**, 15537–15544 (2019).

Author contributions

C.H.S. Nkimbeng wrote the manuscript and performed the simulations. H. Wang designed and measured the fabricated prototype. H. Lee analysed the simulation and measurement results. Y. B. Park addressed technical concerns regarding the measurement of the fabricated prototype and supervised the study. I. Park conceived the idea, revised the manuscript, and supervised the study.

Declarations

Competing interests

The authors declare no competing interests.

Additional information

Correspondence and requests for materials should be addressed to Y.B.P. or I.P.

Reprints and permissions information is available at www.nature.com/reprints.

Publisher's note Springer Nature remains neutral with regard to jurisdictional claims in published maps and institutional affiliations.